Environmental Implications of Saline Efflorescence Associated with Metallic Mining Waste in a Mediterranean Region

Luis Alberto Alcolea-Rubio [1], **Ana Vanessa Caparrós-Ríos** [1], **Virginia Robles-Arenas** [2], **Cristóbal García-García** [2], **Gregorio García** [3], **Rocío Millán** [4], **Araceli Pérez-Sanz** [5] **and Roberto Rodríguez-Pacheco** [6,*]

1   Servicio de Apoyo a la Investigación Tecnológica (SAIT), Technical University of Cartagena (UPCT), 30202 Cartagena, Spain
2   Departamento de Ingeniería Minera y Civil, Technical University of Cartagena (UPCT), 30202 Cartagena, Spain
3   Agronomical Engineering Department, Technical University of Cartagena (UPCT), 30202 Cartagena, Spain
4   CIEMAT, Avenida Complutense 40, 28040 Madrid, Spain
5   Department of Agricultural Chemistry and Food Science, Autonomous University of Madrid (UAM), 28049 Madrid, Spain
6   Spanish National Research Council (CSIC) CN-IGME, Ríos Rosa 23, 28003 Madrid, Spain
*   Correspondence: roberto.rodriguez@igme.es; Tel.: +34-917287235

Abstract: Salt efflorescences from metal sulphides and their waste are important drivers of pollution both in and around mining areas. However, little is known about these supergene minerals, particularly in the mining areas of the Mediterranean. This study aims to characterise saline efflorescences and their leachates from a Mediterranean mining area located in Southeast Spain. The physico-chemical characteristics were determined using stereomicroscopy and compositional analysis, with the following techniques: XRD, WDXRF and TG-MS. Additionally, to assess the risk and potential mobility of their analytes, the samples were subjected to the leaching test DIN 38414-S4. The results showed that the salt efflorescences presented a wide range of crystalline habits and colours. Sulphates were by far the largest mineral group, followed by silicates, oxides and sulphides. Their geochemistry was dominated by elements such as S or Fe, although other potentially toxic elements such as Cd, As, Zn, Pb, Ni and Cu were also present. Due to their high metal(loid) concentrations, the salt crusts studied may act as sources of environmental contaminants, demonstrating that their leachates pose a considerable risk to soil and drinking water quality. An analysis of the correlations and provenances of the components of the salt efflorescences revealed the possible presence of some rare supergene minerals of great interest, such as cuprocopiapite and Pb-As-jarosite.

Keywords: salt crusts; mineralogy; geochemistry; leaching experiments; metal and metalloids; Cartagena-La Unión mining area; Spain

1. Introduction

Environmental impacts in former metal mining areas are often connected to the occurrence of hazardous elements [1]. Due to their porosity and high concentration of metals and metalloids, the mining dumps lead to the capillary rise of water rich in solutes (mainly sulphates and several types of elements) and its subsequent evaporation [1–4]. The solutes can precipitate to form supergene minerals and saline efflorescence crusts on the surface of mining impoundments.

Acid mine drainage (AMD) is produced by the oxidation of mine residues and sulphide minerals, mainly pyrite and other minerals such as galena, sphalerite, etc. The dissolved salts generated in the oxidation processes are at the base of important environmental pollution processes [1,5–7]. The pollution is mainly produced by decreasing pH values of the drainage water and as a consequence of the dissolution of polluting elements, such as some metals and metalloids [1,8,9]. Once these acidic drainage waters precipitate due to

dewatering or a change in their physicochemical characteristics, a series of supergene or secondary minerals are formed, consisting mainly of oxyhydroxides and sulphates [1,5,7]. The type and characteristics of the supergene minerals depend both on the characteristics of the new medium and the pathway followed for the formation of these mineral phases [5,9]. Thus, these secondary minerals can form as saline efflorescences in rocks, tailings and soils by drying the water, by precipitation within water bodies saturated in salts and mine water elements and also by the formation of consolidated crusts and hardpans formed in tailings and mine deposits [1,4,6,10].

On the other hand, the physicochemical characteristics, but the mineralogy of the supergene minerals above all, will vary depending on the mineralogy of the parent materials and the type of generated waste [5,11]. Thus, they can form from oxyhydroxides and oxyhydrosulphates such as goethite and jarosite, among others, to sulphates of different elements that give rise to gypsum, melanterite, copiapite, halotrichite or epsomite, to other mineral phases that are generally rich in metals and of low crystallinity [1,2,10].

These supergene minerals are of great importance for sequestering and/or mobilising potentially toxic elements (PTEs) to the extent that they can promote co-precipitation or stable sink processes of PTES, even by regulating the pH of mine water, influencing the mobility of metals and metalloids [1,8,9]. Concerning this role of secondary minerals, it is worth noting the behaviour of saline efflorescences which, normally having high solubility, are likely to easily release their associated elements, some of them with toxic effects, which makes the salt crusts agents very effective against contamination in mining environments and its surroundings [9,12].

Secondary minerals can be spread by wind and water or washed away to infiltrate and cause groundwater pollution. The occurrence and environmental significance of salt crusts and efflorescences in mine tailings have been recently studied [1–4,13]. Mine impoundments are backfills of fine-grained materials produced during differential flotation treatments of metallurgical materials. These materials are characterised by slow drying processes and, at the same time, rapid water saturation [14–17], as well as significant capillary processes due to their high porosity and fine texture [17–19]. The presence of salt crusts and efflorescence is characteristic of the metal sulphide mining waste deposits. In this sense, what is decisive is the presence of a variable porosity that allows the capillary movement of water, loaded with mineral salts and metallic sulphates that end up evaporating on the surface and generating secondary mineral deposits [11,17,20]. In this respect, column test studies conducted under laboratory conditions are used to evaluate the desiccation, hydraulic and geochemical evolution of these supergene minerals [14,17,21–27].

The direct study of the hydromechanical properties of mining waste is not an easy approach, so this type of research under field conditions is not very common, although some studies have been carried out in the field during the last decades [28,29]. One of these cited studies has even come to experimentally assess the chemical and geological changes that occur during the evaporation in the capillaries and pore water of metal sulphide mine tailings [23]. Salt efflorescences have been referred to by some authors as water-soluble precipitates, they function as temporary traps for toxic metals and metalloids (metal(loid)s). However, the situation could change drastically and suddenly if the entire load of PTEs were to be released due to a change in environmental conditions. This could affect deep areas, such as aquifers, through infiltration, and/or be dispersed over the surface by wind and runoff during heavy rainfall events, resulting in a variety of environmental impacts on soils and water bodies.

The tailings, mineralogy and several environmental aspects associated with the former mining district of Cartagena-La Unión, in Southeast Spain, have been extensively investigated during the last three decades [30–33]. However, the characteristics of saline efflorescences in these environments have barely been considered in these studies. The present study aims to fill this gap in the knowledge of these supergene minerals of high environmental value and significance. Therefore, this study aims to describe and characterise the secondary minerals known as salt efflorescences, as well as their leachates, from an area

affected by former mining activities. In addition, the correlations between the components and factors that affect these salt crusts have been evaluated, as well as the possible origin of the elements present in these supergene mineral phases.

2. Materials and Methods

2.1. Study Area

The survey area is in the former mining district of Cartagena-La Unión, located in the Region of Murcia, in the southeastern area of the Iberian Peninsula (Spain) (Figure 1).
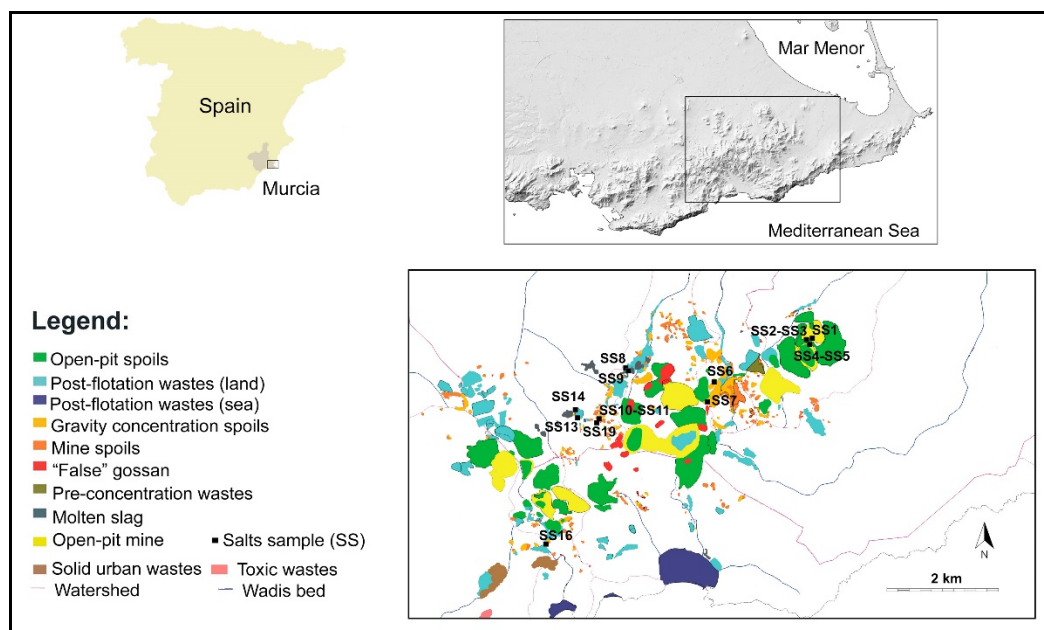
Figure 1. Distribution of the 15 sampling sites (SS) where specimens of salt efflorescences were collected. Modified from [31].

The Sierra Minera de Cartagena-La Unión is located on the northeastern edge of the Cordilleras Beticas, in Southern Spain. The mountains are parallel to the coast in an approximately east-west direction. In this zone, there are two alpine thrusts: the Nevado-Filabride unit, which is older, and the Alpujarride unit, which is more recent and located above the previous one [30,33]. Both the Nevado-Filabride unit, which is formed by medium-grade metamorphic series, and the Alpujarride unit, which shows lesser grade metamorphism, are composed of thick carbonate layers interstratified with detrital series [30,31,33]. In the central part of this mining area, some calc-alkaline magmatic stocks were intruded during the Miocene, with magmas of intermediate to rhyodacitic composition accompanied by magmatic dykes and breccias [30,31,33]. From a morphological point of view, the types of mineralisation enriched in metals and metalloids are distributed among the geological mantles, both of silicates and pyrites, and the dissemination of Miocene materials and the vein and stockwork structures are associated with the vulcanites [30,33]. In turn, the metallic mineral deposits in this area have originated from magmatic processes that have taken place throughout the geological history of the Baetic Basin. These processes include pre-orogenic magmatism, probably from the Late Triassic or Jurassic, followed by post-orogenic magmatism in the post-Miocene and from which most metal sulphide deposits result from hydrothermal processes [30,33].

This area covers approximately 50 km^2. Argentiferous galena (PbS, Ag), sphalerite (ZnS) and pyrite (FeS) have been mined from the 3rd century BC until 1991 AD [30,31]. Today, this former mining area is made up of some 89 large tailings and flotation waste, and a plethora of smaller tailing piles of different types that make up over 2300 tailing sites scattered throughout the mining area [32]. A large part of the hundreds of millions

of tons of metallic sulphides, limestone and other geological materials extracted over centuries are distributed among all these deposits, of which some 350 million tons were mobilised in the last 20th century alone [32]. This exploitation gave rise to the mobilisation of metals and metalloids such as Zn, As, Cd and Pb as the most important elements from an environmental point of view, along with others such as Ni, Cu, and Sb, among others [20]. This has resulted in a dangerous environmental situation, insofar as the PTEs associated with these tailings generate supergene mineral phases in the form of saline efflorescences that affect both the population and the ecosystems surrounding the mining area.

According to the Köppen climate classification, this area has a "steppe or sub-desert Mediterranean" climate. Average winter temperatures are above 10 °C, summers are very hot with average temperatures above 26 °C, average annual temperatures are above 18 °C and rainfall does not exceed 300 mm per year and is concentrated in spring and autumn [34,35].

2.2. Salt Efflorescence Sampling

To obtain a representative sample of the salt efflorescences, fifteen strategic sampling sites (SS) were selected throughout the area (Figure 1). Sampling campaigns were carried out carefully, collecting the salt crusts from the surface of different mining wastes. These samples were carefully packed in plastic bags and stored in the laboratory for further analysis.

To avoid peak broadening and amorphousness in mineralogical and geochemical analysis, samples were air-dried for 24 h and thoroughly hand-ground in a mortar and pestle to obtain a final particle size of less than 100 μm.

2.3. Stereomicroscopy for Macroscopic Characterisation of Samples

This technique allows small magnifications of relatively large objects to produce a three-dimensional display of the sample. It has a long working distance that facilities sample handling during observation. This makes it a key tool to appreciate the appearance of the particles that make up the mineral under study.

Samples were previously conditioned at 60 °C overnight to release most of their moisture. Then, around 30 mg of each sample was spread, albeit with some pressure note white double-sided adhesive tape, which can hold up to four samples per assembly. After each sample was placed, the tape was blown to ideally maintain a monolayer of particles. The colour of salt crusts has been determined using Munsell colour charts [36].

Finally, the samples were visualised in a stereoscopic microscope (SZ61 TR, Olympus, Tokyo, Japan), at a working distance of 110 mm and 20–45× magnification, using LED illumination. Images were captured in a 1600 × 1200 format using a digital camera (Leica MC190 HD, Wetzlar, Germany) and the Leica Application Suite software (v.4.8.0, 2015) (Leica Microsystems, Heerbrugg, Switzerland).

2.4. Mineralogical Composition of Salt Efflorescences

A Bruker D8 Advance θ-θ mode instrument (Bruker Corporation, Billerica, MA, USA) with a 2° windowed one-dimensional detector and CuK radiation (40 kV, 30 mA) was used to study the mineralogy of the powdered salt crusts. To avoid peak broadening and amorphousness, the samples were air-dried for 24 h and thoroughly hand-ground in a mortar and pestle to a final particle size of less than 100 μm. This means that the stable phases were the main focus of the results. For the investigation of efflorescence minerals, collection and storage using a specific approach were required [8]. Stepped intervals of 0.05° were used to scan powder samples from 5 to 70° in 2θ while rotating them at 30 rpm. Processed samples were mounted in a rear-loading plastic sample container. XRD patterns (DIFFRAC.EVA 3.0, Bruker AXS, 2012, and the PDF-4 + powder diffraction file database ICDD, 2013) allowed us to identify the main crystalline phases of the compounds.

In addition, the stability, hydration status and the presence of non-mineral phases in the minerals have been studied by thermogravimetry. Thermogravimetric analysis is a powerful tool for characterising material thermal stability by monitoring the weight change

that occurs as a sample is heated at a constant rate. In this sense, it is commonly used to determine mineral stability, degradation temperature and thermal decomposition and to monitor the mass change by mass spectrometry [8]. Therefore, the thermal stability of these mineral assemblages under oxygen gas was determined by thermogravimetry-mass spectrometry analysis (TG-MS) using a Mettler Toledo TGA/DSC 1HT (Mettler Toledo, Küsnacht, Switzerland). Thermogravimetric analysis has also proven to be effective in estimating H_2O content, organic matter content, SO_3 content and residue content.

The geological materials studied include sulphides, silicates, oxides, hydrated sulphates and organic debris. When the powdered sample of these materials was heated to 30 to 1075 °C, it was possible to examine the stages of loss of the various components by thermogravimetry coupled with mass spectrometry. The final thermogram for each material studied will result from the sum of the decomposition profile of each of its components.

2.5. Geochemistry of the Salt Efflorescences

Samples for wavelength dispersive X-ray fluorescence spectrometry (WDXRF) were properly prepared according to the procedure described at the beginning of this section. The loss-on-ignition (LOI) method was used to estimate H_2O and CO_2 contents and thus give a quantitative estimation of the elemental composition of the mineral samples. Loss-on-ignition estimation was made based on the previously TG-MS analysis.

As part of the sample processing, approximately 10 g of the sample was used to create pressed powder granules. The materials were perfectly pelletised with high moisture content and mixed without any binder. Due to the scarcity of certified reference materials with metal(loid) contents in the same range as the efflorescences examined, a non-standard method was used to analyse the recorded spectra.

A commercial X-ray fluorescence spectrometer (Bruker S4 Pioneer, Bruker AXS GmbH, Karlsruhe, Germany) was used to analyse the samples for geochemical analysis. This device was fitted with an anti-cathode Rh X-ray tube (20–60 kV, 5–150 mA and 4 kW maximum). The analysis was carried out in vacuum mode, which allowed for improved detection in low Z cases, minimising losses due to air absorption. The recorded spectra were analysed using commercial software (Bruker-AXS and Socabim's commercial software SpectraPLUS, EVA 1.7, Bruker AXS GmbH, Karlsruhe, Germany, 2006), applying the fundamental parameter technique. The CO_2 and H_2O contents were evaluated by thermogravimetric analysis (TG-MS) for semi-quantitative evaluation by WDXRF.

Finally, PTEs (Zn, Pb, Sb, Co, Cr, Ni, As, Cu and Cd) enrichment in salt efflorescences was analysed. The enrichment factor (EF) provided by [20] was used to calculate the enrichment of metal(loid)s in salt efflorescences compared to soil:

$$EF = [\text{metal(loid) in salt efflorescence mg/kg}]/[\text{metal(loid) in soil mg/kg}]$$

2.6. Salt Leaching Experiments

The real environmental impact of heavy metal(loid)s was assessed by salt leaching studies. To determine the leachability in water (DIN 38414-S4 [37], 5 g of salt efflorescence samples were poured into polypropylene tubes with 50 mL of purified water. Then, the tubes were closed and shaken for 24 h at room temperature. The undissolved residue was removed by filtration after the 24 h leaching period using a 0.45 μm pore size filtration membrane that had been pre-washed with water. Finally, pH values were measured in the extracts, as well as electrical conductivity (EC), total dissolved solids (TDS), the concentration of other selected cations and anions, and metals and metalloids. Ion concentration was measured using Ion chromatography (Metrohm 850 Professional IC, Metrohm, Herisau, Switzerland) and metal(loid) concentration was determined by ICP-MS (Agilent 7900 ICP-MS, Agilent Technologies, Tokyo, Japan).

Additionally, the enrichment of Zn, Pb, Sb, Co, Cr, Ni, As, Cu and Cd in the leachates was analysed in comparison with the natural soils of the area, according to the enrichment factor (EF) provided by [20].

A Ficklin diagram was generated to categorise the leachates obtained from the leaching tests [38–40]. The Ficklin diagram is often used to analyse chemical changes in mineral solutions of different origins. It is a scatterplot that shows the pH value against the total concentration of the potentially toxic elements considered in this research, mainly Zn, As, Cd and Pb, but also Ni and Cu. These elements were chosen over the more commonly used metals, such as Fe, Al and Mn because they have proven to be the best indicators of different geological conditions. The different geological controls can be distinguished by differences in the sum of the concentrations of these elements considered for different samples.

2.7. Multivariate Statistical Analyses

The Kolmogorov–Smirnov test was performed to validate the normality of the data. Multivariate analyses of the gathered data were conducted with the statistical program IBM SPSS version 20 (IBM, Armonk, NY, USA).

This statistical study considered 15 efflorescences of sulphate salts and their leachates. The soil parameters included the potentially toxic elements obtained from WDXRF analysis (Zn, As, Cd, Pb, Ni and Cu,) and the sum of all elements. The most common sulphate minerals present in the studied samples (divalent metal sulphate minerals, halotrichite group minerals, copiapite group minerals and jarosite group minerals) determined by XRD were also included. Finally, several variables related to salt efflorescences and their leachates such as H_2O, O.M., pH, EC, Cl^- and SO_4^{2-} have been evaluated. Thus, the statistical treatment combines geochemical and hydrochemical data, i.e., the mineral deposit and its drainage signature. The product-moment correlation coefficient (Pearson) for each pair of variables was entered into the matrix. Statistical significance levels were expressed at 0.05 level (2-tailed).

After obtaining individual component loadings, a principal component analysis (PCA) was carried out in IBM SPSS Statistics 20 to analyse the relationship between the measured values. A varimax rotation and a z-transformation were performed to reduce the dimensions of the standardised variables into other principal components [41,42]. In this way, this technique achieves multiple sets of results by grouping some variables and eliminating others of lesser importance. Before this analysis, the data matrix adequacy was assessed using Bartlett's test of sphericity and the Kaiser–Meyer–Olkin (KMO) test. In addition, the communality values have been taken into account as a criterion to eliminate those variables with extraction values lower than 0.5 [41–43]. This technique is used to distinguish between anthropogenic and natural sources and to better understand the correlations between the variables under research. These statistical analyses define the relationship between salt efflorescences and physicochemical variables for better interpretation of salt crust mineralogy and its origin. It is a strong and practical statistical tool.

3. Results and Discussion

3.1. Macroscopic Characterisation by Stereomicroscopy

Supergene minerals were identified from the mining waste deposits. They were composed of ochre-coloured precipitates, efflorescent salts and other weathered geological types that underlie these secondary sulphate minerals, of which sulphides make up a significant component of stony materials. The general appearance of the different salt efflorescences is shown in Figure 2 both at the time of collection and under the stereomicroscope a few days later. Many of the salt samples were taken from exposed vertical surfaces facing north, which were shielded from both sunlight and rainfall, protecting them from dramatic fluctuations in humidity and temperature.

Figure 2. Two stereo microscopic observations of the salt efflorescences evaluated in this work are shown on the right, along with sampling sites (on the left). Images on the right have a 40× magnification and are scaled to 500 μm long. SS1 (**a**), SS2 (**b**), SS3 (**c**), SS4 (**d**), SS5 (**e**), SS6 (**f**), SS7 (**g**), SS8 (**h**), SS9 (**i**), SS10 (**j**), SS11 (**k**), SS12 (**l**), SS13 (**m**), SS14 (**n**), SS15 (**o**).

According to Munsell notation [36], the colour of the salt efflorescences powder included: pale yellow (SS1: 2.5Y 8/2; SS3: 5Y 8/2; SS10: 5Y 7/3), very pale yellow (SS11: 2.5Y 9/2), light greenish grey (SS2: GLEY 1 8/1), pale brown (SS4: 2.5Y 7/4; SS15: 2.5Y 8/4), very pale brown (SS13: 10YR 7/4), light yellowish brown (SS5: 10YR 6/4; SS6: 2.5Y 6/4), light brown (SS7: 7.5YR 6/3), reddish brown (SS8: 2.5YR 5/3), pale olive (SS9: 5Y 6/3), white (SS12: 2.5Y 9.5/1) and pinkish white (SS14: 7.5YR 8/2).

Depending on the metal (loid) and its oxidation state, and therefore due to charge transfer transitions and d-d transitions, these saline minerals can show different colours. Under the optical microscope, a plethora of crystalline habits was discovered, including equant crystals, needle-like or hairy salts, pseudocubes, fibre bundles, fish-scale morphologies and crust-like aggregates.

3.2. Mineralogy of the Salt Efflorescences

The semiquantitative estimations for the samples' crystalline percentages are listed in Table 1. Data are based on the relative intensity ratio (RIR) approach. Since many precipitates generated in this context were weakly crystalline, computed amorphousness was also provided. On the other hand, the salt efflorescences that form there are also rich in heavy metals and metalloids because the sulphide mine tailings are metalliferous. Sulphates (57.7–100%, average 85.1%), silicates (maximum value 27.2%, average 8.5%) and other binary compounds such as oxides and sulphides (up to 15.9%, average 6.5%) were also detected. The amorphousness ranged from 9.4 to 28.9%, with an average of 17.2%.

Table 1. Mineral compounds identified by XRD in the salt efflorescences analysed. Semi-quantitative analysis (wt.%). H_2O, O.M., SO_3 and residue content (%) by TG-MS.

Mineral	General Formula	SS1	SS2	SS3	SS4	SS5	SS6	SS7	SS8	SS9	SS10	SS11	SS12	SS13	SS14	SS15
Sulphates group		81	80	74	84	58	81	83	86	79	87	98	100	89	97	100
Bianchite	$ZnSO_4 \cdot 6H_2O$	13	0	0	0	0	0	0	0	0	0	0	0	0	0	0
Goslarite	$ZnSO_4 \cdot 7H_2O$	1	0	0	0	0	0	0	0	0	0	0	0	0	0	0
Gunningite	$ZnSO_4 \cdot H_2O$	7	0	7	0	0	0	0	0	0	0	0	0	0	0	3
Gypsum	$CaSO_4 \cdot 2H_2O$	4	3	2	77	54	2	12	11	4	3	<1	<1	2	<1	1
Hexahydrite	$MgSO_4 \cdot 6H_2O$	21	0	31	0	0	0	53	40	75	84	0	0	51	52	0
Melanterite	$FeSO_4 \cdot 7H_2O$	0	0	0	0	0	0	0	0	0	0	0	0	7	0	0
Rozenite	$FeSO_4 \cdot 4H_2O$	0	0	0	0	0	11	0	0	0	0	0	0	0	0	0
Starkeyite	$MgSO_4 \cdot 4H_2O$	32	0	0	0	0	41	0	0	0	0	0	0	0	0	0
Halotrichite	$FeAl_2(SO_4)_4 \cdot 22H_2O$	3	0	0	0	0	0	0	0	0	0	89	0	28	0	0
Apjohnite	$MnAl_2(SO_4)_4 \cdot 22H_2O$	0	0	34	0	0	0	0	0	0	0	0	0	0	0	0
Dietrichite	$ZnAl_2(SO_4)_4 \cdot 22H_2O$	0	0	0	0	0	9	0	0	0	0	0	0	0	0	0
Pickeringite	$MgAl_2(SO_4)_4 \cdot 22H_2O$	0	77	0	0	0	0	0	25	0	0	0	100	0	45	0
Copiapite	$Fe_2{+}Fe_3{+}4(SO_4)_6(OH)_2 \cdot 20H_2O$	0	0	0	0	0	0	0	0	0	0	0	0	0	0	13
Magnesiocopiapite	$MgFe_4(SO_4)_6(OH)_2 \cdot 20H_2O$	0	0	0	0	0	0	4	0	0	0	0	0	1	0	79
Jarosite	$KFe3(SO4)2(OH)6$	0	0	0	0	0	0	0	0	0	0	0	0	0	0	4
Hydroniumjarosite	$(H_3O)Fe_3(SO_4)_2(OH)_6$	0	0	0	0	0	18	0	0	0	0	0	0	0	0	0
Natrojarosite	$NaFe_3(SO_4)_2(OH)_6$	0	0	0	7	4	0	0	0	0	0	0	0	0	0	0
Plumbojarosite	$PbFe_6(SO_4)_4(OH)_{12}$	0	0	0	0	0	0	14	10	0	0	0	0	0	0	0
Botryogen	$MgFe(SO_4)_2(OH) \cdot 7H_2O$	0	0	0	0	0	0	0	0	0	0	7	0	0	0	0
Slavikite	$NaMg_2Fe_3{+}5(SO_4)_7(OH)_6 \cdot 33H_2O$	0	0	0	0	0	0	0	0	0	0	2	0	0	0	0
Silicates group		19	20	14	14	27	3	5	<1	6	5	2	0	7	3	0
Greenalite	$(Fe^{2+},Fe^{3+})_2{-}3Si_2O_5(OH)_4$	0	5	2	1	2	2	3	0	5	4	0	0	1	0	0
Hornblende	$(Ca,Na)_2{-}3(Mg,Fe,Al)_5(Al,Si)_8O_{22}(OH,F)_2$	0	0	0	4	4	0	0	0	0	0	0	0	0	0	0
Kaolinite	$Al_2Si_2O_5(OH)_4$	10	0	2	0	0	0	0	0	0	0	2	0	0	1	0
Muscovite	$KAl_2(AlSi_3O_{10}(OH,F)_2$	9	15	10	9	21	1	1	<1	1	0	0	0	6	2	0
Vermiculite	$(Mg, Fe^{2+})_3(Al,Si)_4O_{10}(OH)_2 \cdot 4H_2O$	<1	0	0	0	0	0	1	0	<1	1	0	0	0	0	0

Table 1. *Cont.*

Mineral	General Formula	SS1	SS2	SS3	SS4	SS5	SS6	SS7	SS8	SS9	SS10	SS11	SS12	SS13	SS14	SS15
Oxides/sulphides group		0	0	12	2	15	16	12	14	15	8	0	0	4	0	0
Hematite	Fe_2O_3	0	0	0	0	0	0	0	5	0	0	0	0	0	0	0
Pyrite	FeS_2	0	0	0	0	0	4	0	0	0	0	0	0	0	0	0
Quartz	SiO_2	0	0	12	2	15	12	12	9	15	8	0	0	4	0	0
Computed amorphousness (%)		20	18	16	9	15	17	29	25	22	16	14	13	13	18	13
H_2O content (%)		12.2	21.0	14.3	10.4	10.6	11.2	9.8	13.6	17.0	15.7	26.8	27.7	9.2	23.0	19.7
Organic matter (OM) content (%)		0	0	0	4.1	3.3	1.3	2.4	0	0	0	0	0	4.3	0	0
SO_3 content (%)		32.8	33.8	30.6	21.9	22.1	34.8	12.5	22.5	27.6	28.6	43.6	44.1	27.1	44.3	40.3
Residue content (%)		54.9	45.1	55.0	63.6	64.0	52.5	75.3	63.9	55.3	55.5	29.5	28.1	59.3	32.6	39.9

These data depict several groups of secondary sulphate minerals. With a maximum of 87% and an average of 47%, the hydrous metal sulphates with divalent cations ($A_2+SO_4 \cdot nH_2O$, with A = Mg, Ca, Mn, Fe, Co, Ni, Cu and Zn; n = 1–7) were the most common. This group was present in every specimen examined, and their crystalline phases are as follows: hexahydrite (averaging 27%), gypsum (averaging 11.8%), starkeyite (only present in SS1 and SS6 and averaging $\leq$ 41%,), gunningite (averaging $\leq$ 7%, found exclusively in SS1, SS3 and SS15), bianchite ($\leq$13%, found exclusively in SS1), rozenite ($\leq$11%, found exclusively in SS6), melanterite ($\leq$7%, found exclusively in SS13) and goslarite ($\leq$1%, found exclusively in SS1). The halotrichite ($AB_2(SO_4)_4 \cdot 22H_2O$, where A = Mg, Mn, FSS^{2+}, Ni and Zn; and B = Al, Cr and FSS^{3+}) and copiapite ($A_2+FSS^{3+}4(SO_4)_6(OH)_2 \cdot 20H_2O$, where group A = Ca, Cu, Fe, Mg and Zn, was also found among the mixed divalent-trivalent hydrated mixed metal sulphates. The second-largest group, halotrichite, reached 100% in SS12 and had an average occurrence of 45.4% among the nine occasions on which its presence was found.

Dietrichite, apjohnite, halotrichite and pickeringite, in increasing order of abundance, represented this group. Copiapite and magnesiocopiapite are present in SS15, SS7 and SS13, respectively. These minerals, which had an overall average of 24.2%, are examples of the copiapite group. The iron hydroxysulphate mineral jarosite group [$AFSS^{3+}3(SO_4)_2(OH)_6$, where A = Na^+, K^+, H_3O^+, Ag^+ and $Pb_2^{+0.5}$] gives the crusts their distinctive ochre hue. In this screening, an average of 9.5% of plumbojarosite, hydroniumjarosite, natrojarosite and jarosite were discovered among the six samples in which their presence was detected. Only SS11 included other sulphates as botryogen and slavikite.

The fact that metallic sulphates behave as true solid solutions is important to note since it suggests that the crystalline phases found by diffraction techniques are end-member phases. Within the range of ionic radii allowed by the crystal lattice, the actual situation involves a significant amount of cation substitution. By way of illustration, SS12 recorded 100% pickeringite, while Fe, Mn and Zn, in decreasing order, substituted for Mg at some specific atomic positions, keeping cell characteristics within the range of pickeringite.

Other substances are transported to the soil surface at the same time as the slowly emerging soluble salts. Muscovite (averaging 5.1%), greenalite (averaging 1.7%), kaolinite (with an average of 1%), hornblende (present only in SS4 and SS5 and averaging $\leq$ 4% in these samples) and vermiculite (present only in SS14, SS7, SS9 and SS10 and averaging $\leq$ 1% in these samples) served as representatives of silicates in this survey. Finally, the remaining components included oxides and sulphides. Averaging 6%, quartz reached 15.4%, while pyrite was only 3.9% present in SS6 and haematite was only present in SS8 at 5%. This wide variety in the mineralogy of salt efflorescences is consistent with the results of previous studies in other mining areas [1–4].

Regarding thermogravimetry-mass spectrometry results, the samples produced three main effluent gases during heating. Dehydration occurred in the thermal range 30–500 °C, with a thermal increase of around 10 °C/min, depending on the amount of free, constitution (or constitutional) and crystalline water, and organic matter. Carbon dioxide loss (decarbonisation) occurred in several steps over 150–650 °C in response to the occurrence of organic matter. Finally, the loss of SO_3 (desulphation) was mostly produced in the range 350–1075 °C, mainly indicating the presence of metallic sulphides and sulphates. Figure 3 depicts an illustration of decomposition in an oxidising environment.
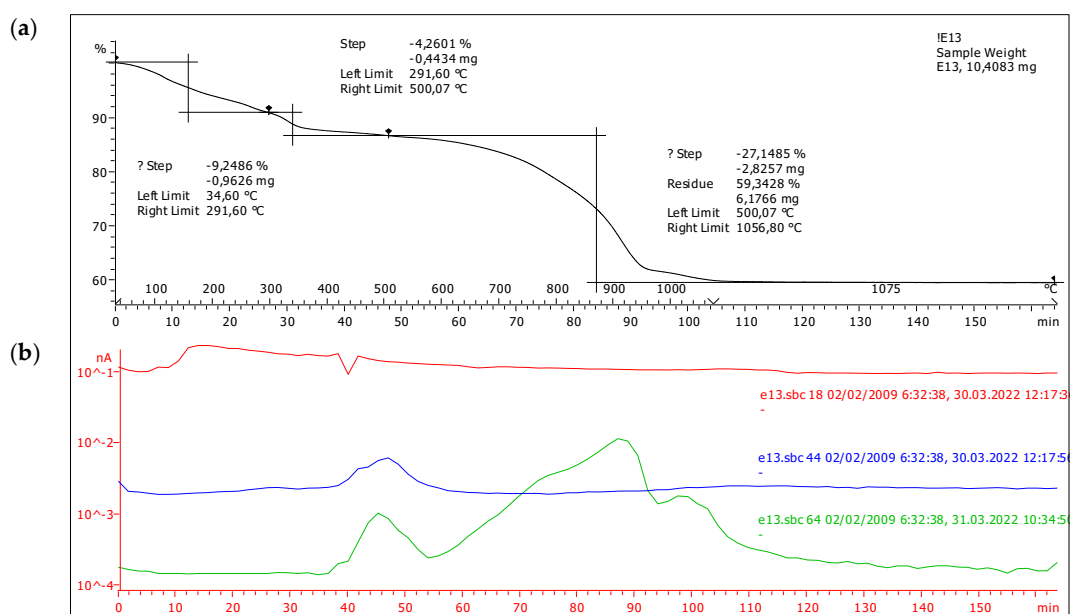
Figure 3. An example of thermogravimetric analysis (for sample SS13): (**a**) thermogram, (**b**) ionic current plot of gases generated during the sample breakdown, where the red line stands for water profile, the blue line for carbon dioxide and the green line for sulphur trioxide (SO_3).

As previously stated, it was difficult to make a detailed and precise assignment of each weight reduction with each decomposition step due to overlap between neighbouring stages, especially when organic matter was present. Data on H_2O, organic matter, SO_3 and residue content are summarised in Table 1.

The average percentage of water percentage was 16.1%, with a range of 9.2 to 27.7%. Without taking into account the combustion of organic matter, the dehydration process can reach temperatures of 150–545 °C. This maximum level was higher in the absence of organic matter and there was more sulphate involved, as well as higher water content.

Organic matter was only found in SS4–SS7 and SS13 and varied from 1.3 to 4.3%, with an average of 3.1 % in the five samples in which it was detected. The temperature range, which was wider in an inverse proportion to the water content, was 150–670 °C. It is recognised that microbiological activity supports the biotic oxidation of sulphides and that AMD environments generally support a thriving microbiome [8].

Sulphide oxidation occurs through an acid-producing process. For this reason, carbonates were hardly found in the salt efflorescence. Additionally, the desulphation of the jarosite mineral group occurs between 500 and 1000 °C [44], and decomposition of the carbonates occurs during this time. If the mass spectrometry study was carried out carelessly, the results could be misinterpreted. As is common in these secondary minerals, sulphur trioxide was the component that evolved in the greatest abundance in the samples. Its content varied between 12.5 and 44.3%, with an average of 31.1%, growing proportionally to the water level, indicating the predominance of hydroxysulphates and/or hydrated sulphates. The overall decomposition temperature ranged from 350 to 1075 °C, so the 1400 °C necessary to decompose all the sulphur present in the samples was not reached. Moreover, due to the collapse of the crystal lattice, part of the SO_3 could have evolved during the final stages of dehydration and/or decarbonisation. In the end, an average SO_3 recovery value in the gaseous form of 88% was found.

The primary components of the final residue produced after burning were oxides and silicates. These fine ashes ranged from 28.1 to 75.3%, averaging 51.6%, and increased in inverse proportion to the SO_3 content.

3.3. Results of the Geochemical Composition of the Salt Efflorescences

In addition, a study of the elemental composition of the salt efflorescence measured by WDXRF and TG-MS (wt.%) was carried out. The loss-on-ignition (LOI) method was used to estimate the water and carbon dioxide contents. Considering only those intensities whose values were greater than several times more than the statistical background, some interesting results have been found. According to Miller & Miller (2010) [45], about three different fractions can be found in minerals. The major fraction contributes between 10 and 100% of the weight of the sample, the minor fraction accounts for 0.1–10% of the total, and a micro fraction has a concentration of between 1 and 1000 ppm. In the major fraction (Table 2), elements such as S and Fe have been found with percentages of 6–19 and 0.7–23, respectively. In the minor fraction, elements such as Mg, Si, Al, Zn, Ca, Mn, Na, Pb, Cl and K were found with percentages ranging from 0.4 to 9.5, 0.1 to 9.4, 0.1 to 7.9, 0.04 to 11, 0.05 to 13, 0.05 to 3.6, 0.03 to 1.9, 0.002 to 2.5, 0.02 to 0.4 and 0.01 to 1.0, respectively. Finally, the elements in the micro fraction were As, Sr, Cd, Ba, Sb, Rb, Ag, Zr, Ti, Cu, P, Ni, Co and Cr, with an approximate concentration expressed in ppm of 1750, 451, 358, 220, 130, 110, 67, 57, 35–1610, 26–1393, 39–270, 19–179, 24–93 and 23–68, respectively. This large quantity and variety of elements, both potentially toxic and non-toxic, is common to salt efflorescences studied in other mining areas [1–4].

According to the WHO [46], these health-relevant PTEs in potable water were a major cause of water contamination due to the high solubility of most of the salt efflorescence minerals. These PTEs include elements such as As, Cd, Ba, Sb, Cu, Ni and Cr, which were present in the micro fraction. In the same situation, elements such as Zn, Pb and Mn were present but in higher concentrations.

In terms of the enrichment of PTEs in the salt efflorescence, significant differences were observed between the different elements (Table 2). The mean PTE values ranged from more than 22690 ppm (Zn) and 4200 ppm (Pb) to approximately 47 ppm (Sb), 49 ppm (Co), 52 ppm (Cr) and 68 ppm (Ni). Other intermediate values were 426 ppm (As), 230 ppm (Cu) and 143 ppm (Cd).

To estimate the enrichment factors, the average enrichment values of the soils in the area in the elements considered were needed (Table 2). The top 60 cm of the soils' typical local background concentrations were derived from [47]. Analytes with EF < 10 (Co = 5, Ni = 3 and Cr = 1) were deemed to be of low enrichment, 10 < EF < 100 (As = 61, Sb = 59 and Cu = 18) suggested mild enhancement, while species with EF > 100 were thought to have a substantial enrichment (Zn = 553, Cd = 477 and Pb = 468). All of this demonstrated that these PTEs are structurally crucial in salt blooms and crusts that are associated with the presence of mining waste, such that they can act as a source of contaminants to the surrounding soil and water.

3.4. Salt Leaching Results

The findings of the leaching tests conducted on the efflorescence of salts are listed in Table 3. As part of Council Decision 2003/33/EC [48,49], which defines standards and practices for the reception of residues at dumpsites (L/S = 10 L/kg; leachate extracted by DIN 38414-S4). This regulation also includes the leaching limit values (LLVs) and total dissolved solids (TDS). The pH regulation levels are given in [38,39], while the EC limit value is obtained from [38]. The leaching tests were carried out at a constant room temperature (25 °C).

Table 2. Ignition weight loss (LOI) and geochemical composition in decreasing order of element concentration of the salt efflorescences determined by TG–MS add WDXRF (wt.%). n.d. not detected. Numbers in brackets after PTEs means enrichment factors (EF) of the salt efflorescences in relation to nearby natural soils.

	SS1	SS2	SS3	SS4	SS5	SS6	SS7	SS8	SS9	SS10	SS11	SS12	SS13	SS14	SS15
LOI	12.29	21.08	14.37	14.41	13.86	12.58	12.11	13.63	17.05	15.79	26.88	27.74	13.51	23.02	19.74
S	14.61	14.6	13.22	14	11.45	15.52	6.089	10.52	12.89	13.71	18.88	18.69	12.32	19.04	16.67
Fe	3.6186	3.3946	3.8766	8.672	16.59	21.2356	23.2756	21.1356	7.9616	8.7996	3.9996	0.7323	13.8456	2.0526	22.1356
Mg	4.06	3.41	3.823	0.436	0.663	2.715	3.374	3.098	7.918	9.517	2.762	3.1	4.648	5.665	0.807
Si	5.117	5.083	7.583	5.598	6.419	3.159	9.443	6.336	7.206	6.511	0.349	1.21	5.912	0.385	0.0898
Al	3.6231	5.6741	5.1561	2.478	2.08	1.3271	2.2671	1.9171	3.4441	2.9131	7.3441	7.8951	2.5571	4.1311	0.1381
Zn (553)	11.44	4.351	5.184	0.2435	0.12	0.7953	1.656	1.112	1.074	0.0417	0.1026	0.0409	2.438	2.523	2.948
Ca	0.553	0.203	0.326	12.98	9.663	0.713	1.172	1.242	0.695	0.71	0.0454	0.151	1.082	0.103	0.305
Mn	2.17	2.225	3.315	0.0493	0.0495	1.292	1.481	0.7658	1.562	0.5475	0.5561	0.6776	3.588	3.582	0.166
Na	1.87	0.64	1.2	0.741	0.233	0.24	0.287	0.359	0.321	0.036	0.03	0.369	0.384	0.259	0.362
Pb (468)	0.7988	0.114	0.0069	0.0839	0.101	0.084	2.471	2.078	0.162	0.004	0.0016	0.005	0.3913	0.0277	0.0063
Cl	0.0786	0.231	0.422	0.0341	0.0565	0.14	0.0845	0.0455	0.0873	0.024	0.021	0.02	0.169	0.032	0.0674
K	0.254	0.279	1.01	0.612	0.449	0.129	0.151	0.121	0.102	0.014	0.012	0.103	0.108	0.011	0.019
As (61)	n.d.	0.0032	n.d.	n.d.	0.021	0.0439	0.0708	0.175	0.0307	0.0449	0.0053	0.0054	0.0778	0.0068	0.0654
Sr	0.007	0.0018	0.0057	0.0451	0.0276	0.0014	0.0029	0.0049	0.0022	0.0025	n.d.	0.0054	0.0025	0.001	0.0012
Cd (477)	0.0346	0.016	0.0042	n.d.	n.d.	n.d.	0.0089	0.0074	0.0066	n.d.	0.0089	n.d.	0.018	0.0358	0.0026
Ba	n.d.	n.d.	0.022	0.013	0.0051	0.0037	n.d.	n.d.	0.002	n.d.	n.d.	n.d.	0.0011	n.d.	n.d.
Sb (59)	0.0016	n.d.	n.d.	n.d.	n.d.	n.d.	0.0088	0.013	0.0014	0.0022	0.0008	n.d.	0.0054	n.d.	n.d.
Rb	n.d.	0.0012	0.0051	0.011	0.0063	0.0004	0.0028	0.002	0.0009	n.d.	0.0002	0.0004	0.0005	n.d.	n.d.
Ag	0.0067	n.d.	n.d.	n.d.	n.d.	n.d.	n.d.	0.0057	n.d.	0.0025	0.0011	n.d.	0.0017	n.d.	n.d.
Zr	0.0015	0.0028	0.0056	0.0057	0.0046	0.0022	0.0027	0.002	0.0036	0.0037	n.d.	0.0016	0.002	0.0002	0.0002
Ti	0.0574	0.0793	0.161	0.109	0.108	0.0482	0.106	0.0967	0.0836	0.116	0.0036	0.0186	0.091	0.0061	0.0035
Cu (18)	0.0118	0.0136	0.0036	0.007	0.0076	0.0078	0.0236	0.0335	0.0304	0.0026	0.0041	0.0031	0.0096	0.0485	0.1393
P	0.019	0.017	0.026	0.024	0.018	0.0094	0.027	0.025	0.021	0.025	0.0056	0.015	0.016	0.0039	0.005
Ni (3)	0.0179	0.0164	0.0095	0.0019	0.002	0.002	0.0041	0.0043	0.004	0.002	0.0051	0.014	0.0095	0.0057	0.0038
Co (5)	0.0024	0.008	0.0032	0.0041	0.0093	0.0033	0.0025	0.0038	0.0025	0.0037	0.0071	0.0074	0.0047	0.003	0.008
Cr (1)	0.0063	0.0065	0.006	0.0052	0.0051	0.0042	0.0062	0.0063	0.0067	0.0068	0.004	0.0034	0.0063	0.0023	0.0033

Table 3. Leaching test results for salt efflorescence samples. SS1 to SS15 are different salt samples. EC = electrical conductivity (expressed in mS/cm), TDS = total dissolved solids (expressed in g/kg). Cd, As, Zn, Pb, Ni, Cu and Sb expressed in mg/kg, SO_4^{2-} and Cl^- (expressed in g/kg). P.p. = Pollution potential according to WHO guidelines for drinking water [46] expressed as number-fold enriched; n.p.r. = no pollution risk. Elements are presented in decreasing order of pollution potential.

	pH	EC	TDS	Cd	As	Zn	Pb	Ni	Cu	Sb	SO_4^{2-}	Cl^-
SS1	4.2	23.0	11.9	18.9	0	6624	3.7	1.3	0.7	2.6	33.7	0
SS2	3.5	23.4	12.0	10.8	0	3439	1.4	8.8	5.8	0.8	46.7	0.1
SS3	3.4	25.7	13.4	2.1	0	3686	0.1	3.9	0.3	0.7	48.7	0.3
SS4	3.4	3.9	2.0	0.4	0	188	0.1	0.2	0.3	0	7.6	0
SS5	2.5	5.5	2.9	0.1	0	96	0.1	0.2	0.1	0	6.8	0
SS6	2.7	24.4	12.6	0.4	0.3	497	0	0.5	2.2	0	39.0	0.1
SS7	4.3	12.2	6.3	4.6	0	628	2.8	0.6	0.1	0	17.1	0
SS8	2.9	18.7	9.7	4.9	0	699	0.2	2.1	8.4	0	29.4	0
SS9	4.1	23.6	12.2	4.3	0.1	660	0.2	1.1	7.3	2.0	35.2	0
SS10	3.8	26.7	13.8	0	0	22	0	0.3	0.1	0	38.0	0
SS11	2.5	24.7	12.8	5.4	0.2	68	0	2.6	1.5	0	56.5	0
SS12	3.0	26.8	13.8	0.3	0.6	27	0	7.3	0.5	0	64.4	0
SS13	4.0	19.8	10.3	9.5	0	1349	2.7	2.6	0.1	0	32.0	0.1
SS14	2.8	29.7	15.2	18.8	0	1781	0	2.6	19.6	0	58.5	0
SS15	2.2	19.6	10.2	2.2	40.9	2298	0	1.9	78.8	29.2	72.3	0.1
P.p.	n.p.r.	2-12	3-25	<6290	<4092	7–2208	<365	2–126	<39	n.p.r.	14–145	n.p.r.

All samples examined did not meet the requirements for residues to be accepted at landfills. Levels of acidity, and the most mobile elements of Zn and Cd, whose mean levels surpassed the leaching limit values (LLV) for the acceptance of waste at hazardous waste landfills, were responsible for it. Taking into account the total ratios of each parameter to that of the WHO drinking water recommendations [45,46] for each sample, the efflorescence can be classified according to their increasing degree of harmfulness as follows: SS5 < SS10 < SS4 < SS12 < SS6 < SS9 < SS8 < SS8 < SS11 < SS7 < SS7 < SS3 < SS13 < SS2 < SS15 < SS14 < SS1. The environmental hazard level was not specifically correlated with any secondary sulphate mineral. All of them may be regarded as harmful; however, the copiapite group's sulphates appeared to act as significant PTEs sinks.

European Council Decision 2003/33/EC [48,49] defines up to three sets for the reception of waste at dumpsites. Set 1 fixes the limit values for the reception of hazardous residues at hazardous waste landfills, while set 2 determines the limit values for the reception of hazardous residues at non-hazardous waste landfills and set 3 states the acceptance limits for inert waste residues landfills. As for the results of the leaching experiments, all pH values exceeded the LLVs regarded for the reception of hazardous residues at non-hazardous waste landfills, while none of them exceeded these limits for EC (Table 3). In turn, for TDS, all values except SS4 and SS5 exceeded the LLVs for the reception of inert residues to inert waste landfills.

On the other hand, the different elements and anions considered in this study showed different behaviours depending on the set considered within Decision 2003/33/EC. The values of set 1 were exceeded for elements such as Zn (SS1-SS3, SS6-SS9 and SS13–SS15), As (SS15), Cd (SS1–SS3, SS7–SS9, SS11 and SS13–SS15), Sb (SS15) and SO_4^{2-} (SS11, SS12, SS14 and SS15). Set 2 cut-off values were found to be close to or above them for Cu (SS15), Zn (SS1–SS9, SS12 and SS13–SS15), As (SS15), Cd (SS10), Sb (SS1–SS3, SS9 and SS15) and SO_4^{2-} (SS1–SS3, SS6 and SS8–SS15). Finally, set 3 limits were crossed for Ni (all values except SS4, SS5 and SS10), Cu (SS2, SS6, SS8, SS9, SS14 and SS15), Zn (all values), As (SS12 and SS15), Cd (all values except SS10), Sb (SS1-SS3, SS9 and SS15), Pb (SS1, SS2, SS7 and SS13) and SO_4^{2-} (all values). In addition, for Cl^-, no LLV value was exceeded.

Another issue to be considered is the drinking water quality. In this regard, the WHO has provided guidelines for drinking water [46]. When comparing the values of those guidelines with the results generated in the leaching tests (Table 3), 1 L of leachate

could normally contaminate up to approximately 2000 L of potable water. In this regard, these parameters can be classified according to their contamination potential, in increasing degree, indicating the level of enrichment for each parameter compared to the WHO guidelines: Cu (39) < EC (2–12) < TDS (3–25) < Ni (2–126) < SO_4^{2-} (14–145) < Pb (365) < Zn (7–2208) < As (4092) < Cd (6290). The samples did not present any risk of pH, and Cl^- and Sb contamination. In addition to the above, another aspect considered was the enrichment in anions and metallic and metalloid elements of the salt efflorescence leachates concerning the presence of metals and other ions in the soils of the mining area [47]. In summary, from the data collected in Table 4, it can be concluded that the percentage of enrichment in metallic elements, metalloids, and anions of these efflorescences concerning the surrounding natural soils can be ordered as follows, in increasing sequence: SS5 < SS10 < SS4 < SS1 < SS7 < SS13 < SS9 < SS6 < SS3 < SS8 < SS8 < SS12 < SS14 < SS2 < SS11 < SS15.

Table 4. Cations and anions enrichment factors percentage of the efflorescence salt leachates relative to nearby natural soils. Elements are presented in decreasing average enrichment.

Sample	SO_4^{2-}	Zn	Cl^-	Cd	Ni	Cu	As	Sb	Pb
SS1	76.9	57.9	33.3	54.5	7.2	6.1	0.6	0.2	0.5
SS2	100	79.0	60.2	67.2	53.6	42.9	1.1	0.3	1.2
SS3	100	71.1	64.1	50.6	40.5	9.3	1.0	0.2	0.8
SS4	18.0	77.2	42.7	59.4	9.2	3.8	0.1	<0.1	0.1
SS5	19.8	80.1	24.5	19.0	9.6	1.2	0.1	<0.1	0.1
SS6	83.7	62.5	55.2	73.0	22.6	27.5	0.7	<0.1	<0.1
SS7	93.4	37.9	37.1	52.1	15.5	0.3	<0.1	<0.1	0.1
SS8	93.2	62.9	54.4	66.8	49.1	25.2	<0.1	<0.1	<0.1
SS9	91.1	61.5	43.4	65.4	27.0	23.9	0.2	0.1	0.1
SS10	92.3	52.9	24.4	0.1	16.5	<0.1	<0.1	<0.1	0.7
SS11	99.7	66.4	93.8	60.8	51.4	37.5	3.6	<0.1	0.3
SS12	100	66.9	94.0	41.3	52.1	17.4	11.4	<0.1	<0.1
SS13	86.7	55.3	62.5	52.7	27.2	3.8	<0.1	<0.1	0.7
SS14	100	70.6	81.7	52.6	46.7	40.3	0.3	<0.1	0.1
SS15	100	78.0	100	84.8	51.1	56.6	62.6	9.7	0.1
Average	83.7	65.3	58.1	53.4	32.0	19.7	5.5	0.7	0.3

In addition, in Table 4 it can be seen how the most abundant chemical species can be displayed in increasing order as follows: Pb < Sb < As < Cu < Ni < Ni < Cd < Cl^- < Zn < SO_4^{2-}. It is noteworthy that Cd can be easily released during the solubilisation of Zn-enriched salt efflorescence. Paradoxically, although these water-soluble salts were in an area with a high presence of Pb and Zn, Pb was less of an environmental problem as it is less mobilised from salt efflorescence. These results are largely in agreement with data from previous studies [2–4].

Complementarily, the different leachates generated by each salt efflorescence were classified using a Ficklin diagram [38–40] (Figure 4).

For this purpose, both the pH values and the sum of metal(loid)s generated in the efflorescence leachates carried out according to the DIN 38414-S4 leaching test were considered. This resulted in a total of four categories of the diagram out of a possible 12. In this respect, four of them (SS4, SS7, SS9 and SS10) were considered as acid low-metal, five of them (SS5, SS6, SS8, SS11 and SS12) were considered as high-acid low-metal, four of them (SS1, SS2, SS3 and SS13) were considered as acid high-metal, while the remaining two (SS14 and SS15) were classified as high-acid high-metal. In summary, about two-thirds were considered low-metal solutions, while the rest of the leachates were categorised as high-metal solutions. Consequently, these leachates can have a significant impact on soil and water quality. In addition, the risk level calculated by adding the proportions of each individual to the WHO guideline limits [46] was found to be consistent with this Ficklin plot.
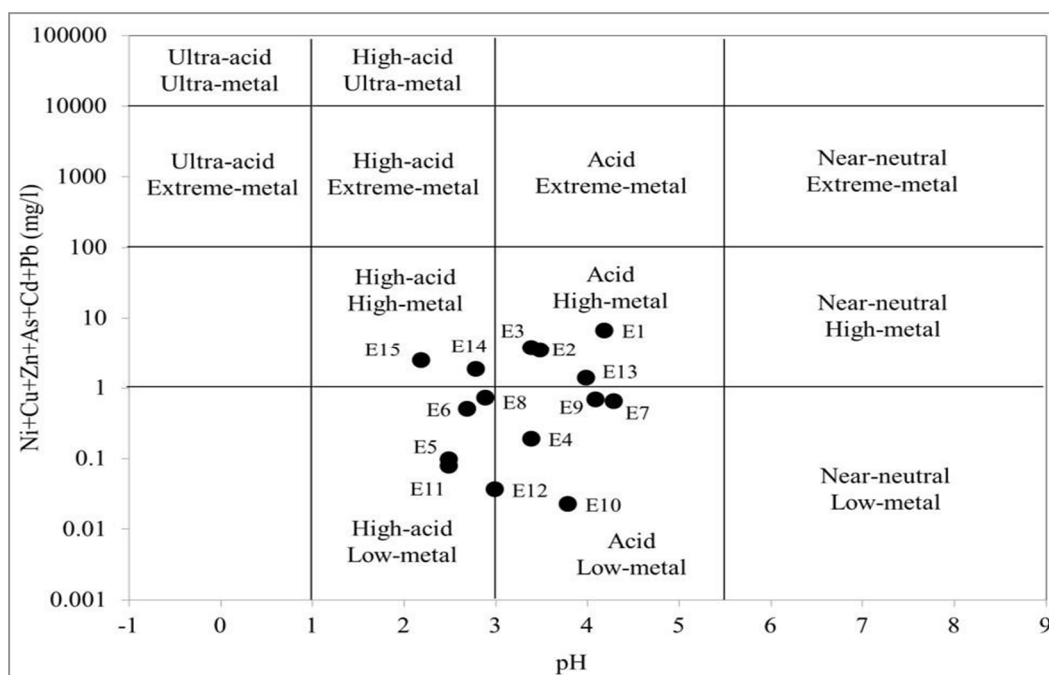
Figure 4. Metal(loid)s with pollution potential according to WHO guidelines for drinking water [46] content of leachates of the studied salt efflorescences: Ficklin diagram.

3.5. Statistical Results

Pearson's correlation test and PCA were used in this statistical study. Using the Kolmogorov–Smirnov test, the hypothesis of the normality of the datasets has been validated.

The Pearson product-moment correlation coefficient was entered for each pair of variables to create the correlation matrix. A two-tailed significance test revealed that the correlations were significant. Usually, there are intricate relationships between various aspects [50]. Data normalisation (Z-score) and Pearson's correlation matrix were used to eliminate multivariate problems and increase the relevance of mineral data [51].

This statistical study took into account 15 salt efflorescences (E) and their leachates (L). Solids-related parameters included TG-MS data (H_2O and organic matter levels), as well as potentially toxic elements from WDXRF analysis and the total of these elements. The main sulphate groups measured by XRD were considered; namely, divalent metal(loid) sulphate minerals with the general formula $A^{2+}SO_4$-nH_2O. Minerals from the copiapite, halotrichite and jarosite groups were considered. Finally, several variables related to saline efflorescence leachates were also considered, including pH, EC, the soluble fraction of the above PTE as determined by ICP-MS, and Cl^- and SO_4^{2-} ion chromatography measurements. Table 5 shows in bold the significant correlations at the 0.05 level between the values (2-tailed).

The halotrichite group minerals showed a substantial positive association with water content because they have the highest amount of crystalline water (22 molecules). On the other hand, minerals from the group of the divalent metal sulphate, with up to seven water molecules in its composition, showed a negative correlation with water. In addition, there were remarkable positive relationships between EC, Ni (L) and SO_4^{2-} concentrations and water content. On the other hand, there were negative significant correlations between organic matter and H_2O, SO_4^{2-} and EC.

Table 5. Correlation matrix of salt efflorescences (E) and their leachates (L). Significant correlations at the 0.05 level are shown in bold. (H_2O is the water content and OM stands for organic matter, both determined by thermogravimetry (TG-MS); E = Salt efflorescence in solid form; L = leachate of salt efflorescence; $\sum M$ = sum of the metal(loid)s considered); Di.Su. = divalent metal(loid) sulphate minerals; Hal. = halotrichite group minerals; Cop. = copiapite group minerals; Jar. = jarosite group minerals.

	H_2O	OM	Ni(E)	Cu(E)	Zn(E)	As(E)	Cd(E)	Pb(E)	$\sum M$(E)	Di.Su.	Hal.	Cop.	Jar.	pH	EC	Ni(L)	Cu(L)	Zn(L)	As(L)	Cd(L)	Pb(L)	$\sum M$(L)	Cl^-	SO_4^{2-}
H_2O	1.00	**−0.66**	0.28	0.17	−0.15	−0.34	0.09	−0.40	−0.24	**−0.73**	**0.79**	0.14	−0.50	−0.42	**0.60**	**0.62**	0.25	−0.08	0.17	0.11	−0.42	−0.08	−0.05	**0.80**
OM		1.00	−0.30	−0.25	−0.26	0.07	−0.18	0.10	−0.23	0.36	−0.36	−0.16	0.30	0.16	**−0.77**	−0.38	−0.27	−0.32	−0.18	−0.21	0.26	−0.32	−0.14	**−0.71**
Ni(E)			1.00	−0.19	**0.71**	−0.33	**0.53**	−0.04	**0.66**	−0.32	0.51	−0.16	−0.48	0.33	0.39	**0.72**	−0.16	**0.72**	−0.15	**0.56**	**0.54**	**0.72**	0.27	0.32
Cu(E)				1.00	0.07	0.29	0.06	0.02	0.09	−0.28	−0.24	**0.92**	0.04	−0.39	0.03	−0.08	**0.98**	0.13	**0.92**	0.07	−0.14	0.14	0.18	0.46
Zn(E)					1.00	−0.23	**0.67**	0.09	**0.97**	0.09	−0.10	0.06	−0.27	0.37	0.23	0.14	0.06	**0.99**	0.06	**0.68**	**0.65**	**0.99**	0.35	0.11
As(E)						1.00	−0.16	**0.67**	−0.04	0.15	0.18	0.47	−0.03	−0.14	−0.25	0.19	−0.26	0.16	−0.15	0.05	−0.26	−0.11	−0.11	−0.17
Cd(E)							1.00	0.12	**0.67**	0.12	−0.16	−0.34	0.29	0.34	0.13	−0.01	−0.14	0.01	−0.15	0.12	0.49	0.01	−0.06	0.15
Pb(E)								1.00	0.34	0.25	−0.25	−0.12	**0.52**	0.36	−0.28	−0.21	−0.14	0.01	−0.15	0.12	0.49	0.01	−0.22	−0.40
$\sum M$(E)									1.00	0.15	−0.17	0.04	−0.12	0.44	0.14	0.08	0.04	**0.93**	0.03	**0.68**	**0.73**	**0.93**	0.28	0.01
Di.Su.										1.00	**−0.77**	−0.38	0.19	**0.60**	−0.27	**−0.72**	−0.38	0.00	−0.39	0.08	0.27	−0.01	−0.32	**−0.69**
Hal.											1.00	−0.22	−0.40	−0.27	0.47	**0.83**	−0.17	−0.05	−0.21	0.14	−0.17	−0.05	0.09	**0.57**
Cop.												1.00	0.03	−0.05	−0.06	−0.42	**0.96**	−0.02	−0.14	−0.14	0.13	−0.31	0.28	0.46
Jar.													1.00	−0.12	−0.39	−0.07	−0.42	−0.48	0.30	−0.35	0.00	−0.31	−0.14	−0.39
pH														1.00	0.00	0.00	−0.07	−0.48	0.30	−0.44	0.27	**0.70**	0.29	−0.40
EC															1.00	0.43	0.07	0.26	−0.03	0.35	−0.10	0.26	0.23	**0.79**
Ni(L)																1.00	−0.01	0.24	0.18	−0.01	0.15	0.24	0.38	**0.54**
Cu(L)																	1.00	0.13	**0.96**	0.01	−0.22	0.15	0.25	**0.54**
Zn(L)																		1.00	0.12	**0.66**	**0.56**	**1.00**	0.45	0.19
As(L)																			1.00	−0.15	−0.17	0.13	0.28	0.48
Cd(L)																				1.00	**0.56**	**0.66**	−0.05	0.17
Pb(L)																					1.00	**0.56**	−0.01	−0.28
$\sum M$(L)																						1.00	0.46	0.20
Cl^-																							1.00	0.34
SO_4^{2-}																								1.00

Positive and significant correlations were found for Zn, Cd, Ni and Cu, with the sum of the set of elements studied ($\sum$M), both in solid and leached form, i.e., all PTEs except those of low leachability (Pb and As). Similarly, Zn, Cd and Ni, and the sum of the PTEs appeared significantly and favourably correlated among themselves. Other significant favourable correlations were found in the copiapite group with Cu in its solid form of sulphate salt efflorescence samples (E) and As in its form of leachates of sulphate salt efflorescence (L), among other correlations. On the other hand, the halotrichite group showed positive correlations with Ni (L) and SO_4^{2-}, as did the jarosite group with Pb (E). The pH also appeared positively correlated with the divalent metal(loid) sulphate minerals group and with Pb (L), as did EC and Ni (L) with SO_4^{2-}, Cu (L) with As (L) and SO_4^{2-}, among others. Interestingly, the Cl^- concentration did not correlate with the remaining parameters. Additionally, the divalent metal(loid) sulphate minerals group showed significant negative correlations with the halotrichite group, Ni (L) and SO_4^{2-}.

Although in previous studies Pb, Cd and Ni had a negative correlation trend with pH [41], in the sense that at low pH values the mobility of these metal ions increases [5], in this case, there is either no significant correlation or it is positive, as in the case of Pb, which may be due to the low pH value in all the samples analysed. On the other hand, although organic matter does not present positive correlations with most of the variables considered, the vast majority of these correlations, especially the significant ones, turn out to be negative, which coincides with what has been indicated by other authors [41].

Significant correlations between minerals and their major (Zn, Pb, etc.) and trace (Cd, As, etc.) elements, such as those found in this research, have been demonstrated by several studies [52,53]. However, in many other aspects, the behaviour of these salt efflorescences differs, at least in part, from that shown by the soils and mining tailings described by other authors. Thus, some significant correlations have been found for primary and secondary minerals, such as those described between Fe-Al oxides with Ni and As [54], between Ni, SO_4, TDS, pH and EC with each other [55] or between pH and SO_4 [56], have not been significant for the supergene minerals considered in this study. However, some described correlations between EC, pH and texture of mining waste sediments that seem to determine the mineralogical composition, dissolution and oxidation processes and their influence on the physicochemical properties and mobility of potentially toxic elements associated with metallic mining waste, may be key in the formation of saline efflorescences from these mining tailings [1,6,9,10,53,57,58]. Similarly, different types of parent materials can generate soils and residues enriched in Ni and Cr [59], while a distinctly clayey and Fe-enriched texture can act to enrich soils in As [60]; something that could explain the presence of these elements in salt crusts present in these environments.

Additionally, a PCA analysis was conducted to quantify all of the mineralogical processes in the research area and to determine the link between the variables in the salt efflorescence. The proportional contribution of each mineral source to the salt crust was determined using this technique.

This statistical procedure is often used to identify and understand the hidden complex and causal relationships between the different properties of the dataset. This is achieved by examining the structure of the data at a smaller scale size and keeping as much variability of the data as possible. It is necessary to estimate the number of principal components in the data to achieve this. The eigenvectors formed by the decomposition of a correlation matrix between pairs of parameters are arranged in order of their associated values. PCA is a mathematical procedure that entails auto-scaling values to create new parameters, computing the covariance matrix and removing elements that only add a small amount of variation to the datasets [8].

When conducting a PCA, the adequacy of sampling must be verified, which requires that the Kaiser–Meyer–Olkin (KMO) test is equal to or greater than 0.50 for the factor arrangement [43]. Furthermore, it is required that the probability related to Bartlett's test of sphericity is not as large as the level of noteworthiness, which translates into the prerequisite that the significance level of Bartlett's test is <0.05 being fulfilled [43]. After

the verification of these two requirements, and therefore being relevant to perform the PCA, the extraction values in the communalities table should be checked in such a way that only those parameters that contribute more than 50% of their variance in the dataset are considered for the PCA test. Varimax with Kaiser normalisation was applied as a rotation method, to ensure that each parameter had a maximum correlation with a single principal component while correlating close to zero with the other elements.

After checking the values of the communalities, it was finally decided to analyse 10 variables with extraction values of the communalities above 0.75, except for one value of 0.66. These 10 variables include the six PTEs considered, in their solid salt form (Ni, Cu, Zn, As, Cd and Pb), and the four groups of supergene minerals considered (divalent metal(loid) sulphate minerals, halotrichite group minerals, copiapite group minerals and jarosite group minerals). These analysed variables should make it possible to unravel the interactions between the different elements under consideration and the secondary minerals. Table 6 shows the PCA results for the variables mentioned above for the salt crust samples studied.

Table 6. Total variance explained and components extracted by principal component analysis.

	Total Variance Explained								
Component	**Initial Eigenvalues**			**Extraction Sums of Squared Loadings**			**Rotation Sums of Squared Loadings**		
	Total	**% of Variance**	**Cumulative %**	**Total**	**% of Variance**	**Cumulative %**	**Total**	**% of Variance**	**Cumulative %**
1	3.187	31.869	31.869	3.187	31.869	31.869	2.433	24.333	24.333
2	2.191	21.915	53.783	2.191	21.915	53.783	2.177	21.770	46.103
3	1.998	19.982	73.765	1.998	19.982	73.765	2.118	21.184	67.287
4	1.346	13.463	87.229	1.346	13.463	87.229	1.994	19.941	87.229
5	0.575	5.749	92.977						
6	0.408	4.081	97.058						
7	0.177	1.775	98.833						
8	0.074	0.737	99.570						
9	0.025	0.249	99.820						
10	0.018	0.180	100.000						

The KMO test measures, among other things, the adequacy of sampling, while Bartlett's test of sphericity indicates the strength of correlation between variables. In this study, the KMO test result met its minimum requirement of being at least equal to 0.5, while Bartlett's test with a significance = 0.000 showed that effective reduction and transformation of the dimensions of the standardised variables can be achieved through PCA. Because of the above, the PCA test with orthogonal varimax rotation was carried out. This methodology has previously been used for similar research purposes by numerous authors [41–43,61].

Four correlated components were extracted by PCA with a total explained variance of more than 87% (Table 6). When all this information is transferred to a graph (Figure 5), it can be determined that component 1 showed a close correlation between metals such as Zn, Cd and Ni. On the other hand, component 2 corresponds to the Cu content which revealed strong relationships with the copiapite group minerals. In turn, component 3 includes the Pb and As contents, which showed a moderate interrelationship with the jarosite group minerals. And, finally, component 4 revealed a strong negative relationship with halotrichite group minerals, but a positive one with divalent metal(loid) sulphate minerals.

Zn, Cd and Ni contents of the salt efflorescences were identified as a component explaining one-third of the total observed variance. In turn, halotrichite minerals and divalent metal(loid) sulphate minerals appeared strongly associated with another component, albeit with different signs.
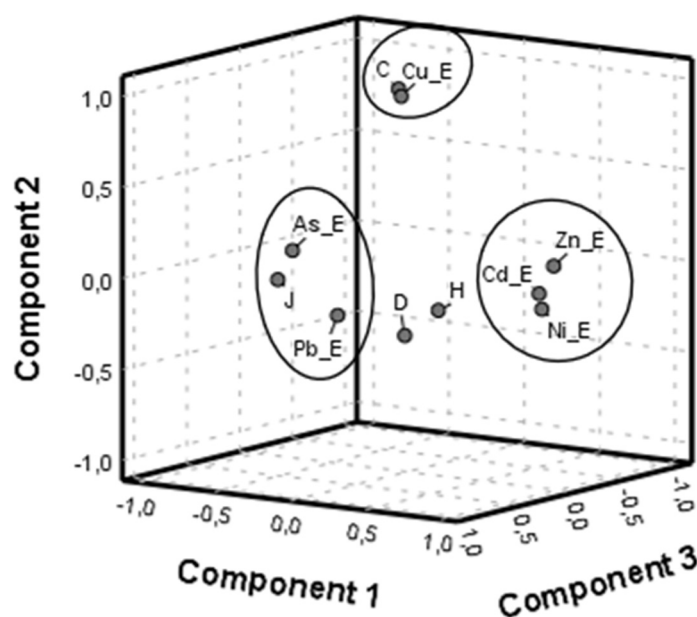
Figure 5. Principal component analysis (PCA) with varimax rotation based on the analysed parameters. PTEs in their salt efflorescence in solid form (E): Ni_E, Cu_E, Zn_E, As_E, Cd_E, Pb_E; D = divalent metal(loid) sulphate minerals; H = halotrichite group minerals; C = copiapite group minerals; J = jarosite group minerals.

Copiapites were an important component for Cu and responsible for a high percentage of the variance, which is consistent with the results observed in the correlation matrix studied above (Table 5). These revealing data suggest that the variant of the copiapite mineral group occurring in the study area may be cuprocopiapite. $(Cu^{2+}Fe^{3+}_{4}(SO_4)_6(OH)_2 \cdot 20H_2O)$. This type of copiapite has traditionally been associated with copper-enriched Chilean mining areas [62]. However, although it is not easy to detect because it usually requires sophisticated techniques such as Raman spectroscopy, it has also been detected in other mining areas in the same mountain range of the study area [12,63]. Consequently, this finding can be considered of great interest and should be taken into account for future mineralogical studies in this area to help confirm this issue.

In addition, jarosite efflorescence shared a major component with Pb and As, results that contrast with previous studies insofar as they related this group of minerals to other distinct elements, such as Fe and Cu [42]. This rare association of jarosite with Pb and As has already been described as a Pb-As-jarosite $((H_3O)_{0.68}Pb_{0.32}Fe_{2.86}(SO_4)_{1.69}(AsO_4)_{0.31}(OH)_{5.59}(H_2O)_{0.41})$ and considered as an analogue of beudantite [64]. The most common version of this mineral is Pb-jarosite, widely described in different environmental conditions [7,65]. In this sense, although this variant of jarosite has never been described for this study area, it has already been mentioned in other mining areas of the same geological complex [66]. Therefore, this finding can also be considered of great interest and should also be taken into account for future mineralogical studies of this mining area.

In addition, the data of this study are in agreement with observations made by other authors, which indicate that during the neoformation of supergene minerals, they trap elements—Pb, Zn, Cd, As and Cu among others—, as well as SO_4^{2-} which are available in mine tailings during dry periods and discharged by dissolution during precipitation events [1,6,9,10,42,53,58,67,68].

4. Conclusions

The salt efflorescences studied showed a wide range of crystalline habits and vibrant colours depending on the metal(loid) and its oxidation state. The most important mineral group are the sulphates, mainly the metal sulphates with divalent cations, but also the halotrichite group, the copiapite group and the jarosite group. Silicates occur in fewer

quantities, followed by oxides and sulphides. Therefore, the major mineral group in these saline efflorescences are sulphates, with a predominance of hydrated sulphates and/or hydroxysulphates.

Regarding the geochemical composition of the salt efflorescences, three different fractions correspond to the majority fraction (S, Fe), a minor fraction (Mg, Si, Al, Zn, Ca, Mn, Na, Pb, Cl, K) and a micro fraction (As, Sr, Cd, Ba, Sb, Rb, Ag, Zr, Ti, Cu, P, Ni, Co, Cr). Relative to soils, potentially toxic elements in the salt efflorescences were particularly high for Zn, Cd and Pb. Other potentially toxic elements such as As and Cu were also present but in lower concentrations. These data reveal that salt efflorescence crust blooms incorporate significant concentrations of heavy metals and metalloids into their structures from mine waste. Therefore, salt efflorescences will have a major impact on soil and water quality. It has been established that the origin of these elements and minerals is mining waste.

In addition, considering the enrichment ratio of the saline efflorescence leachates concerning the presence of metals and other ions in the soils of the mining area, SO_4^{2-} and Zn showed significantly higher values than the rest of the elements, while Pb showed the lowest value. This is paradoxical since the salt crusts in this area show high values of Zn but also of Pb, which indicates that this lower environmental risk of Pb may be due to its lower mobilisation by salt efflorescence. Furthermore, according to the Ficklin diagram performed, approximately 60% of these leachates can be considered as solutions with low metal content, and only the remaining 40% as leachates with high metal content. Salt efflorescences leaching tests revealed that all these salt crusts were found to be too toxic for landfill waste acceptance and could be considered a hazard to soils and drinking water quality according to World Health Organisation guidelines.

Finally, several correlations and common sources have been determined for different PTEs and supergene mineral groups. In this sense, the most remarkable findings have been the association of Cu with copiapites and of Pb and As with jarosites, indicating for the first time in this ancient mining district the possible and relevant presence of cuprocopiapite and Pb-As-jarosite as an analogue of beudantite, respectively, in this mining area.

Author Contributions: Conceptualisation, L.A.A.-R. and R.R.-P.; methodology, L.A.A.-R., C.G.-G., V.R.-A. and A.V.C.-R.; software, L.A.A.-R., C.G.-G. and V.R.-A.; validation, L.A.A.-R. and A.V.C.-R.; formal analysis, L.A.A.-R., G.G. and R.R.-P.; investigation, L.A.A.-R., R.R.-P., R.M. and A.P.-S.; resources, R.R.-P., G.G. and C.G.-G.; data curation, L.A.A.-R. and A.V.C.-R.; writing—original draft preparation, G.G. and R.R.-P.; writing—review and editing, G.G., R.R.-P., L.A.A.-R., R.M. and A.P.-S.; visualisation, R.R.-P. and L.A.A.-R.; supervision, R.R.-P. and L.A.A.-R.; project administration, R.R.-P., L.A.A.-R. and C.G.-G.; funding acquisition, R.R.-P., G.G., R.M., A.P.-S and L.A.A.-R. All authors have read and agreed to the published version of the manuscript.

Funding: This research received no external funding.

Data Availability Statement: Not applicable.

Acknowledgments: The authors gratefully acknowledge the infrastructure support of the Assistance Service for Technological Research at the Universidad Politécnica de Cartagena (Spain). The authors also thank Anna Mateu for revising the language of this manuscript.

Conflicts of Interest: The authors declare no conflict of interest.

References

1. Jambor, J.L.; Nordstrom, D.K.; Alpers, C.N. Metal-sulfate salts from sulfide mineral oxidation. *Rev. Mineral. Geochem.* **2000**, *40*, 303–350. [CrossRef]
2. Buckby, T.; Black, S.; Coleman, M.L.; Hodson, E. Fe-sulphate-rich evaporative mineral precipitates from the Río Tinto, southwest Spain. *Mineral. Mag.* **2003**, *67*, 263–278. [CrossRef]
3. Romero, A.; Gonzalez, I.; Galan, E. The role of efflorescent sulfates in the storage of trace elements in stream waters polluted by acid mine drainage: The case of Peña del Hierro, southwestern Spain. *Can. Mineral.* **2006**, *44*, 1431–1446. [CrossRef]
4. Cala-Rivero, V.; Arranz-González, J.C.; Rodríguez-Gómez, V.; Fernández-Naranjo, F.J.; Vadillo-Fernández, L. A preliminary study of the formation of efflorescent sulfate salts in abandoned mining areas with a view to their harvesting and subsequent recovery of copper. *Miner. Eng.* **2018**, *129*, 37–40. [CrossRef]

5. Alloway, B.J. Sources of Heavy Metals and Metalloids in Soils. In *Heavy Metals in Soils: Trace Metals and Metalloids in Soils and Their Bioavailability*; Alloway, B.J., Ed.; Environmental Pollution; Springer: Dordrecht, The Netherlands, 2012; Volume 22, pp. 11–50.

6. Murray, J.; Kirschbaum, A.; Dold, B.; Mendes Guimaraes, E.; Pannunzio Miner, E. Jarosite versus soluble iron-sulfate formation and their role in acid mine drainage formation at the Pan de Azúcar mine tailings (Zn-Pb-Ag), NW Argentina. *Minerals* **2014**, *4*, 477–502. [CrossRef]

7. Cogram, P. *Jarosite. Reference Module in Earth Systems and Environmental Sciences*; Elsevier: Amsterdam, The Netherlands, 2018.

8. Lottermoser, B.G. *Mine Wastes: Characterization, Treatment and Environmental Impacts*, 3rd ed.; Springer: Berlin/Heidelberg, Germany, 2010; 400p.

9. Hammarstrom, J.M.; Seal Ii, R.R.; Meier, A.L.; Kornfeld, J.M. Secondary sulfate minerals associated with acid drainage in the eastern US: Recycling of metals and acidity in surficial environments. *Chem. Geol.* **2005**, *215*, 407–431. [CrossRef]

10. Carbone, C.; Dinelli, E.; Marescotti, P.; Gasparotto, G.; Lucchetti, G. The role of AMD secondary minerals in controlling environmental pollution: Indications from bulk leaching tests. *J. Geochem. Explor.* **2013**, *132*, 188–200. [CrossRef]

11. Dold, B. Evolution of acid mine drainage formation in sulphidic mine tailings. *Minerals* **2014**, *4*, 621–641. [CrossRef]

12. Sobron, P.; Sanz, A.; Acosta, T.; Rull, F. A Raman spectral study of stream waters and efflorescent salts in Rio Tinto, Spain. *Spectrochim. Acta Part A Mol. Biomol. Spectrosc.* **2009**, *71*, 1678–1682. [CrossRef]

13. Mees, F.; Tursina, T.V. Salt minerals in saline soils and salt crusts. In *Interpretation of Micromorphological Features of Soils and Regoliths*; Elsevier: Amsterdam, The Netherlands, 2018; pp. 289–321. [CrossRef]

14. Rodríguez, R. Estudio Experimental de Flujo y Transporte de Cromo, Níquel y Manganeso en Residuos de la Zona Minera de Moa (Cuba): Influencia del Comportamiento Hidromecánico. Ph.D. Thesis, Polytechnic University of Cataluña, Barcelona, Spain, 2002; pp. 1–457. (In Spanish).

15. Rodríguez, R. Hydrogeotechnical characterization of a metallurgical waste. *Can. Geotech. J.* **2006**, *43*, 1042–1060. [CrossRef]

16. Rodríguez, R.; Candela, L.; Lloret, A. Experimental system for studying the hydromechanical behaviour of porous media. *Vadose Zone J.* **2004**, *4*, 345–353. [CrossRef]

17. Rodríguez, R.; Muñoz-Moreno, A.; Caparrós, A.; García-García, C.; Brime-Barrios, A.; Arranz-González, J.C.; Rodríguez-Gómez, V.; Fernández-Naranjo, F.J.; Alcolea, A. How to Prevent Flow Failures in Tailings Dams. *Mine Water Environ.* **2021**, *40*, 83–112. [CrossRef]

18. Oldecop, L.A.; Rodríguez, R. Estabilidad y seguridad de depósitos de residuos mineros. In *Los Residuos Minero Metalúrgicos en el Medio Ambiente*; Rodríguez, R., García-Cortés, A., Eds.; IGME: Madrid, Spain, 2006; pp. 197–243.

19. Zandarín, M.T.; Oldecop, L.; Rodríguez, R.; Zabala, F. The role of capillary water in the stability of tailing dams. *Eng. Geol.* **2009**, *105*, 108–118. [CrossRef]

20. Carmona, D.M.; Faz Cano, A.; Arocena, J.M. Cadmium, copper, lead, and zinc in secondary sulfate minerals in soils of mined areas in Southeast Spain. *Geoderma* **2009**, *150*, 150–157. [CrossRef]

21. Fujiyasu, Y.; Fahey, M. Experimental study of evaporation from saline tailings. *J. Geotech. Geoenviron. Eng.* **2000**, *126*, 18–27. [CrossRef]

22. Rodríguez, R.; Sánchez, M.; Ledesma, A.; Lloret, A. Experimental and numerical analysis of desiccation of a mining waste. *Can. Geotech. J.* **2007**, *44*, 644–658. [CrossRef]

23. Acero, P.; Ayora, C.; Carrera, J. Coupled thermal, hydraulic and geochemical evolution of pyritic tailings in unsaturated column experiments. *Geochim. Cosmochim. Acta* **2007**, *71*, 5325–5338. [CrossRef]

24. Fisseha, B.; Bryan, R.; Simms, P. Evaporation, unsaturated flow, and salt accumulation in multilayer deposits of paste gold tailings. *J. Geotech. Geoenvironmental Eng.* **2010**, *136*, 1703–1712. [CrossRef]

25. Innocent-Bemard, T. Evaporation, Cracking, and Salinity in a Thickened Oil Sands Tailings. Master's Thesis, Department of Civil and Environmental Engineering, Carleton University, Ottawa, ON, USA, 2013; pp. 1–122.

26. Yao, Y. Dewatering Behaviour of Fine Oil Sands Tailings. An Experimental Study. Ph.D. Thesis, Technische Universiteit Delft, Delft, The Netherlands, 2016; pp. 125–134.

27. Garino, L.M.; Oldecop, L.A.; Romero, E.E.; Rodríguez-Pacheco, R.L. Tailings desiccation process studied in environmental chamber experiment. *Proc. Inst. Civ. Eng.-Geotech. Eng.* **2022**, *175*, 261–271. [CrossRef]

28. Newson, T.A.; Fahey, M. Measurement of evaporation from saline tailings storages. *Eng. Geol.* **2003**, *70*, 217–233. [CrossRef]

29. Blanco, A.; Lloret, A.; Carrera, J.; Olivella, S. Thermo-hydraulic behaviour of the vadose zone in sulphide tailings at Iberian Pyrite Belt: Waste characterization, monitoring and modelling. *Eng. Geol.* **2013**, *165*, 154–170. [CrossRef]

30. Oen, I.S.; Fernandez, J.C.; Manteca, J.I. The Lead-Zinc and associated ores of La Unión, Sierra de Cartagena, Spain. *Econ. Geol.* **1975**, *70*, 1259–1278. [CrossRef]

31. Robles-Arenas, V.M.; Rodríguez, R.; García, C.; Manteca, J.I.; Candela, L. Sulphide-mining impacts in the physical environment: Sierra de Cartagena-La Unión (SE Spain) case study. *Environ. Geol.* **2006**, *51*, 57–64. [CrossRef]

32. García, C. Impacto y Riesgo Ambiental de los Residuos Minero-Metalúrgicos de la Sierra de Cartagena-La Unión (Murcia-España). Ph.D. Thesis, Universidad Politécnica de Cartagena, Murcia, Spain, 2004.

33. Manteca Martínez, J.I.; Ovejero Zappino, G. Los yacimientos Zn, Pb, Ag-Fe del distrito minero de La Unión-Cartagena, Bética Oriental. In *Recursos Minerales de España*; CSIC: Madrid, Spain, 1992; pp. 1085–1102.

34. Capel Molina, J. *El Clima de la Península Ibérica*; Editorial Arial: Barcelona, Spain, 2000.

35. Gil-Guirado, S.; Pérez-Morales, A. Variabilidad climática y patrones termopluviométricos en Murcia (1863–2017). Técnicas de análisis climático en un contexto de cambio global. *Investig. Geográficas* **2019**, *71*, 27–54. [CrossRef]
36. *Munsell Soil Color Charts*; Munsell Color X-Rite: Grand Rapids, MI, USA, 2000.
37. *DIN 38414-S4*; German Standard Methods for the Examination of Water, Waste Water and Sludge; Sludge and Sediments (Group S); Determination of Leachability by Water (S 4). Deutsches Institut fur Normung: Berlin, Germany, 1984; pp. 464–475.
38. Marguí, E.; Hidalgo, M.; Queralt, I.; Rodríguez, R. Métodos de evaluación del riesgo ambiental de los residuos minero-metalúrgicos sólidos. In *Los Residuos Minero-Metalúrgicos en el Medio Ambiente*; Rodríguez, R., García Cortés, A., Eds.; IGME: Madrid, Spain, 2006; pp. 413–439.
39. Perera, A.S.R.; Al-Tabbaa, A.; Reid, J.M.; Stegemann, J.A. State of practice report. UK Stabilisation/Solidification Treatment and Remediation. Part IV: Testing and Performance Criteria. In Proceedings of the International Conference on Stabilization/Solidification Treatment and Remediation, Cambridge, UK, 12–13 April 2005; Balkema: London, UK, 2005; pp. 415–435.
40. Vialle, C.; Sablayrolles, C.; Lovera, M.; Jacob, S.; Huau, M.C.; Montrejaud-Vignoles, M. Monitoring of water quality from roof runoff: Interpretation using multivariate analysis. *Water Res.* **2011**, *45*, 3765–3775. [CrossRef]
41. Chowdhury, A.; Maiti, S.K. Identification of metal tolerant plant species in mangrove ecosystem by using community study and multivariate analysis: A case study from Indian Sunderban. *Environ. Earth Sci.* **2016**, *75*, 744. [CrossRef]
42. Trifi, M.; Gasmi, A.; Carbone, C.; Majzlan, J.; Nasri, N.; Dermech, M.; Charef, A.; Elfil, H. Machine learning-based prediction of toxic metals concentration in an acid mine drainage environment, northern Tunisia. *Environ. Sci. Pollut. Res.* **2022**, *29*, 87490–87508. [CrossRef] [PubMed]
43. Abdullah, S.; Ismail, M.; Ahmed, A.N. Identification of air pollution potential sources through principal component analysis (PCA). *Int. J. Civ. Eng. Technol.* **2018**, *9*, 1435–1442.
44. Frost, R.L.; Weier, M.L.; Martens, W. Thermal decomposition of jarosites of potassium, sodium and lead. *J. Therm. Anal. Calorim.* **2005**, *82*, 115–118. [CrossRef]
45. Miller, J.N.; Miller, J.C. *Statistics and Chemometrics for Analytical Chemistry*; Prentice Hall: Harlow, UK, 2010; 278p.
46. WHO. *Guidelines for Drinking-Water Quality*, 4th ed.; World Health Organisation: Geneva, Switzerland, 2011.
47. Martínez-Sánchez, M.J.; Pérez-Sirvent, C. *Niveles de Fondo y Niveles Genéricos de Referencia de Metales Pesados en Suelos de la Región de Murcia*; Comunidad Autónoma de la Región de Murcia: Murcia, Spain, 2007.
48. Council of the European Union. European Council Decision of 19 December 2002 on establish criteria and procedures for the acceptance of waste at landfills pursuant to Article 16 of and Annex II to Directive 1999/31/EC. *Off. J. Eur. Communities* **2003**, *L11*, 27–49. Available online: http://europa.int/eur-lex (accessed on 25 October 2022).
49. European Commission. *Critical Raw Materials for the EU*; Report of the RMSG Ad-Hoc Working Group on Defining Critical Raw Materials; European Commission: Brussels, Belgium, 2010.
50. Han, J.; Cheng, H.; Xin, D.; Yan, X. Frequent pattern mining: Current status and future directions. *Data Min. Knowl. Discov.* **2007**, *15*, 55–86. [CrossRef]
51. Koklu, R.; Sengorur, B.; Topal, B. Water quality assessment using multivariate statistical methods—A case study: Melen River system (Turkey). *Water Resour. Manag.* **2010**, *24*, 959–978. [CrossRef]
52. Stefanov, S.H.; Ouchev, A. *Gisement Plombo-Zincifère de Sidi Driss*; Rapport Géol. Avec Estimation de Réserves, Rapport Interne; Office National des Mines de Tunisie: Tunis, Tunisia, 1972.
53. Trifi, M.; Dermech, M.; Abdelkrim, C.; Azouzi, R.; Hjiri, B. Extraction procedures of toxic and mobile heavy metal fraction from complex mineralogical tailings affected by acid mine drainage. *Arab. J. Geosci.* **2018**, *11*, 328. [CrossRef]
54. Zhang, H.; Yin, S.; Chen, Y.; Shao, S.; Wu, J.; Fan, M.; Chen, F.; Gao, C. Machine learning-based source identification and spatial prediction of heavy metals in soil in a rapid urbanization area, eastern China. *J. Clean. Prod.* **2020**, *273*, 122858. [CrossRef]
55. Gholami, R.; Kamkar-Rouhani, A.; Doulati Ardejani, F.; Maleki, S. Prediction of toxic metals concentration using artificial intelligence techniques. *Appl. Water Sci.* **2011**, *1*, 125–134. [CrossRef]
56. Rooki, R.; Doulati Ardejani, F.; Aryafar, A.; Bani Asadi, A. Prediction of heavy metals in acid mine drainage using artificial neural network from the Shur River of the Sarcheshmeh porphyry copper mine, Southeast Iran. *Environ. Earth Sci.* **2011**, *64*, 1303–1316. [CrossRef]
57. Dold, B. Element flows associated with marine shore mine tailings deposits. *Environ. Sci. Technol.* **2006**, *40*, 752–758. [CrossRef]
58. Trifi, M.; Charef, A.; Dermech, M.; Azouzi, R.; Chalghoum, A.; Hjiri, B.; Sassi, M.B. Trend evolution of physicochemical parameters and metals mobility in acidic and complex mine tailings long exposed to severe Mediterranean climatic conditions: Sidi Driss tailings case (NW-Tunisia). *J. Afr. Earth Sci.* **2019**, *158*, 103509. [CrossRef]
59. Hu, Y.; Cheng, H. Application of stochastic models in identification and apportionment of heavy metal pollution sources in the surface soils of a large-scale region. *Environ. Sci. Technol.* **2013**, *47*, 3752–3760. [CrossRef]
60. García-Sánchez, A.; Alastuey, A.; Querol, X. Heavy metal adsorption by different minerals: Application to the remediation of polluted soils. *Sci. Total Environ.* **1999**, *242*, 179–188. [CrossRef]
61. Rahman, M.S.; Saha, N.; Molla, A.H. Potential ecological risk assessment of heavy metal contamination in sediment and water body around Dhaka export processing zone Bangladesh. *Environ. Earth Sci.* **2014**, *71*, 2293–2308. [CrossRef]
62. Bandy, M.C. Mineralogy of three sulphate deposits of northern Chile. *Am. Mineral. J. Earth Planet. Mater.* **1938**, *23*, 669–760.

63. Chemtob, S.M.; Arvidson, R.E.; Fernández-Remolar, D.C.; Amils, R.; Morris, R.V.; Ming, D.W.; Prieto-Ballesteros, O.; Mustard, J.F.; Hutchison, L.; Stein, T.C.; et al. Identification of hydrated sulfates collected in the northern Rio Tinto valley by reflectance and Raman spectroscopy. In Proceedings of the 37th Lunar and Planetary Science Conference, Houston, TX, USA, 13–17 March 2006.

64. Hudson-Edwards, K.A. Uptake and release of arsenic and antimony in alunite-jarosite and beudantite group minerals. *Am. Mineral. J. Earth Planet. Mater.* **2019**, *104*, 633–640. [CrossRef]

65. Dutrizac, J.E.; Jambor, J.L. Formation and characterization of argentojarosite and plumbojarosite and their relevance to metallurgical processing. In *Applied Mineralogy: Proceedings of the Second International Congress on Applied Mineralogy in the Minerals Industry, Los Angeles, CA, USA, 22–25 February 1984*; Park, W.C., Hausen, D.M., Hagni, R.D., Eds.; The Metallurgical Society of AIME (the American Institute of Mining, Metallurgical and Petroleum Engineers, Inc.): Warrendale, PA, USA, 1984.

66. Roca, A.; Viñals, J.; Arranz, M.Y.; Calero, J. Characterization and alkaline decomposition/cyanidation of beudantite–jarosite materials from Rio Tinto gossan ores. *Can. Metall. Q.* **1999**, *38*, 93–103. [CrossRef]

67. Dutrizac, J.E.; Jambor, J.L. Jarosites and their application in hydrometallurgy. In *Sulphate Minerals: Crystallography, Geochemistry, and Environmental Significance*; Alpers, C.N., Jambor, J.L., Nordstrom, D.K., Eds.; Reviews in Mineralogy and Geochemistry, 40; Mineralogical Society of America: Chantilly, VA, USA, 2000; pp. 405–443.

68. Gieré, R.; Sidenko, N.V.; Lazareva, E.V. The role of secondary minerals in controlling the migration of arsenic and metals from high-sulfide wastes (Berikul gold mine, Siberia). *Appl. Geochem.* **2003**, *18*, 1347–1359. [CrossRef]